Fractal rigidity of the wheel-rail contact

IOP Conf. Series: Materials Science and Engineering **997** (2020) 012002 doi:10.1088/1757-899X/997/1/012002

Fractal rigidity of the wheel-rail contact

L M Babici[1,2], A Tudor[1], J Romeu Garbi[2] and M Stoica[1]

[1]Department of Machine Elements and Tribology, Polytechnic University of Bucharest, Bucharest, Romania
[2]Acoustical and Mechanical Engineering Laboratory (LEAM), Polytechnic University of Catalonia, Terrassa (Barcelona), Spain

E-mail: lbabici@yahoo.com

Abstract. One of the essential parameters of the roughness with effects on the vibration of the wheel and the rail is the contact stiffness. This rigidity considers the geometry and material of the wheel and rail, which are considered elastic. Also, the micro-geometry of the roughness and the load on the wheel, with elastic, elastoplastic and plastic deformations, depending on the deterministic or random character of the roughness were considered. The dependence of the stiffness on the deformation state of the roughness may explain the different amplitude of the vertical vibrations at the same force on the wheel and the same height of the roughness, but one roughness with different fractal parameters. For the analysis of the dynamic forces in contact, the continuous and underived analytical function that modelled the roughness measured experimentally on the rail was applied.

1.Introduction

An essential parameter for describing the features of the interface in different engineering applications, including wheel-wheel contact, is the stiffness contact.

In this paper, different models are employed to predict the contact stiffness between the wheel-rail roughness using statistical parameters and the fractals.

The contact stiffness at the wheel/rail contact is caused by elastic deformation, which causes a contact area, the size of which increases as the normal load increases. Therefore, the load-deflection relation is non-linear.

In other words, the normal contact stiffness between the wheel and rail as a function of normal load can be approached using a power law, in which the coefficient and power are associated to wheel-rail surface roughness parameters, material properties and the nominal contact area.

2. Surface rigidity with roughness

Contact stiffness is a fundamental parameter for describing the interface characteristics between wheel-rail contact and present an indispensable effect on both the static and dynamic behaviour of the mechanism system, such as contact pressure distribution, vibration, contact area, and interface modelling [1-5].

Referring to the modelling of roughness surface, the statistical approach is one of the most popular methods and different asperity micro-contact statistical models have been proposed.

2.1. Greenwood and Williamson model

Greenwood and Williamson (GW) have developed for the first time the basic elastic contact model based on the elastic Hertzian solution for the roughness surface contact. In their model, were neglected both, the plastic and elastoplastic deformation of asperities. In Greenwood and Williamson model, the roughness surface is described by means of asperities with spherical summits and an identical radius of curvature and the asperity height after a Gaussian form and also, the distribution of peaks has a Gaussian form.[1-3,6].

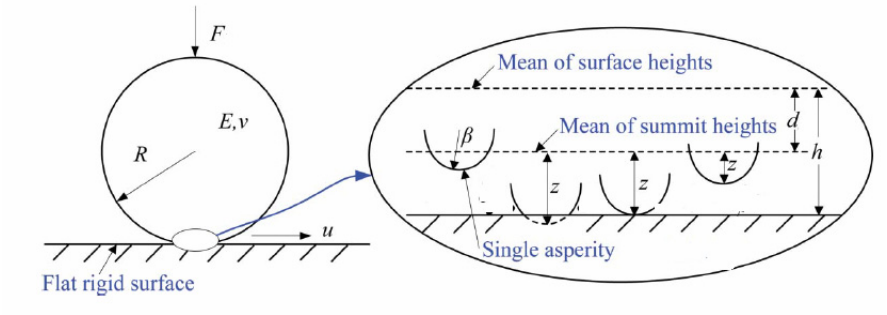

Figure 1. The equivalent contact of a wheel-rail roughness contact region (Xiao, 2018).

The normal contact force of the roughness interface could be obtained as:

$$W_{GW} = N_r \int_h^\infty f_a \Phi_s(s) ds \tag{1}$$

where, N_r represent the number of asperities, $N_r = \eta A_n$, with η that show the asperity distribution density and A_n is nominal contact area. So, the contact force f_a become

$$f_a = \frac{4}{3} E_p \beta^{1/2} \sigma^{3/2} \tag{2}$$

in which, E_p is effective modulus of elasticity, β represents the effective radius of asperities and σ is the standard deviation of the height distribution. These three parameters, σ, β and η are defined in GW model, and are connected to the surface topography.

Therefore, the total load become:

$$W_{GW} = \frac{4}{3} \eta A_n E_p \beta^{1/2} \sigma^{3/2} \int_h^\infty (s-h)^{3/2} \phi_s(s) ds \tag{3}$$

For the contact surfaces of the wheel and rail having a gaussian distribution of heights of asperities, this gives:

$\Phi_s = \exp(-s)$, where Φ_s is height distribution scaled and $E_p = \frac{E}{1-\nu^2}$, with E is Young's modulus and ν is Poisson's ratio.

In this model, was shown that the relationship between A_n and W_{GW} was directly proportional, even if it was supposed that the deformation was considered only elastic.

Introducing the following dimensionless parameters:

$$W_{sGW} = \frac{W_{GW}}{A_n \cdot E_p}, \quad \eta = \frac{N_r}{A_n}, \quad \beta_s = \frac{\beta}{\sqrt{A_n}}, \quad \sigma_s = \frac{\sigma}{\sqrt{A_n}} \tag{4}$$

where N_r is the ratio of peaks to ordinates, and the normal contact stiffness is explained as $K_n = \frac{dW}{d\delta}$.

Considering that $h = \frac{d}{\sigma} = s - \frac{\delta}{\sigma}$, where h represents the height distribution scale, d is separation between wheel and rail, consequently, $K_n = \frac{dW}{d\delta}\frac{dh}{d\sigma}$, then the contact stiffness of the wheel-rail roughness is expressed in the following form

$$K_n = N_r \int_h^\infty K_a \phi_s(s) ds \tag{5}$$

with $K_a = 2E_p(\beta\sigma)^{1/2}$, where K_a represent the contact stiffness with one asperity. Therefore, the express of contact stiffness become

$$K_{nGW} = 2\eta A_n E_p (\beta\sigma)^{1/2} \int_h^\infty (s-h)^{1/2} \phi_s(s) ds \tag{6}$$

Dimensionless normal rigidity of roughness surface is defined

$$K_{sn} = \frac{K_n}{E_p (A_n)^{1/2}} \tag{7}$$

Then, from equations (6) and (7) the express of contact stiffness is:

$$K_{snGW} = 2N_r E_p (\beta\sigma)^{1/2} \int_h^\infty (s-h)^{1/2} \phi_s(s) ds \tag{8}$$

These calculations are achieved by measuring the surface roughness of one sample wheel and rail surface with $E_1 = E_2 = 2{,}1\text{x}10^{11}$, $\nu_1 = \nu_2 = 0.3$). The effects of η, β, σ parameters are observed in figures 2. The dimensionless roughness parameters of rail and wheel parameters are: $\beta_{srw} = 0.015$, $\sigma_{srw} = 0.015$ and $N_{rw} = 608.8$.

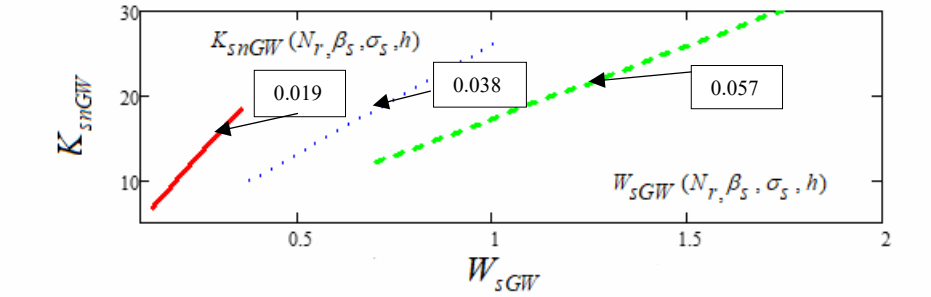

Figure 2a. Normal stiffness versus normal load for three standard deviations: ——— $\sigma_{srw} = 0.019$, - - - - - - - - $2\sigma_{srw}$, - - - - - - - - $3\sigma_{srw}$

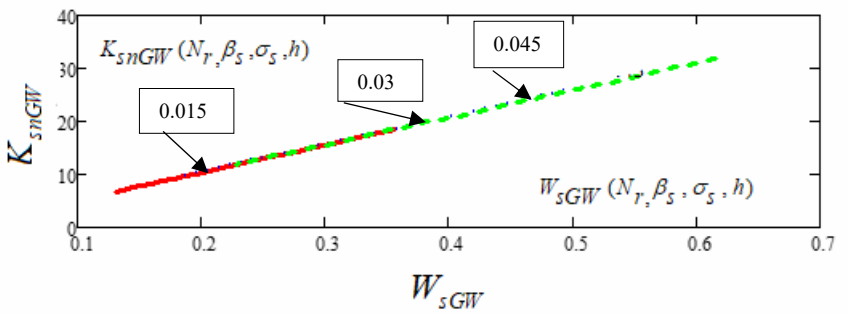

Figure 2b. Normal stiffness versus normal load for three radii of curvature ——— $\beta_s = 0.015$, - - - - - - - - $2\beta_s$, - - - - - - - - $3\beta_s$.

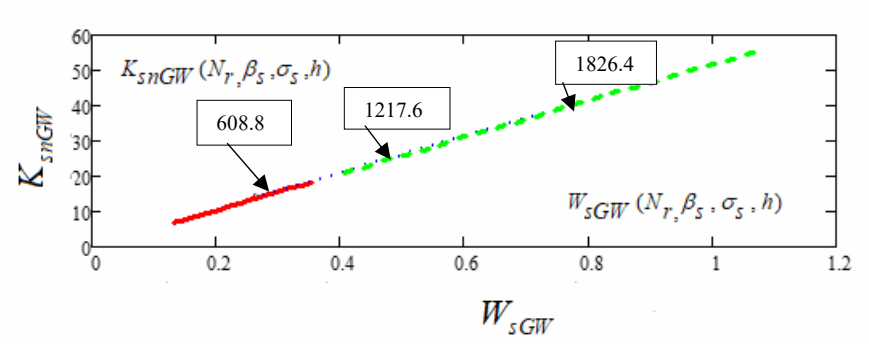

Figure 2 c. Normal stiffness versus normal load for three relative roughness densities: ——— N_{rw}=608.8, - - - - - - - - $2N_{rw}$, - - - - - - - - $3N_{rw.}$

2.2. Onions and Archard model

This model is based on the theory of Whitehouse and Archard [7,8]. In this model, the impact a curvature asperity distribution is detected. In principle, when normal load growing, the contact stiffness growing, too. The research has shown that the surface roughness parameters of the wheel-rail contacting surfaces have very significant effects on the contact stiffness.

The approach gives a distribution of peak curvatures which is dependent upon their height. Unlike the GW model, the Onions and Archard (OA) model contours the surface profile in terms of two parameters, that represents the standard deviation of the height distribution (σ) and correlation distance (τ).

The theory examines a three-dimensional surface, where a peak is defined as the highest point among the five from five points nearby. Consequently, the total load is given as:

$$W_{OA} = \frac{4}{3}\eta(\tau) A_n E_p (\frac{2}{3}\tau)\sigma F(h) ds \tag{9}$$

where,

$F(h) = \int_h^\infty (s-h)^{3/2} \int_0^\infty \frac{f_s(s,C)}{NC^{1/2}} dC ds$, and C is dimensionless asperity curvature

$$f_s(s,C) = \frac{1}{2^{3/2}\pi}\exp(\frac{-s^2}{2})\exp\left[-\left(s-\frac{C}{2}\right)^2\right] erf\left(\frac{C}{2}\right)$$, where

$$erf(y) = \frac{2}{\pi^{1/2}}\int_0^y \exp(-x^2)dx$$ is the error function (10)

In this theory, has considered that $N = 1/3$ represent ratio of peaks to ordinates, for “three point” method, and

$$\eta(\tau) = \frac{1}{5}\frac{1}{(2.3\tau)^2}, \quad \beta = \frac{2}{\pi^{1/2}}\frac{(2.3\tau)^2}{9\sigma} \tag{11}$$

Through dimensionless the following parameters:

$W_{sOA} = \frac{W_{OA}}{A_n E_p}$, $\tau_s = \frac{\tau}{A_n^{1/2}}$ and $\sigma_s = \frac{\sigma}{A_n^{1/2}}$, the dimensionless normal force become (12)

The dimensionless normal contact stiffness after Whitehouse and Archard, could be written:

$$K_{snOA} = \frac{6}{5(2.3\tau_s)} \int_h^{\infty} (s-h)^{1/2} \int_0^{\infty} \frac{f_s(s,C)}{C^{1/2}} dCds \tag{13}$$

It is exemplified in figure 3 and the rigidity variation for three correlation distance (τ).

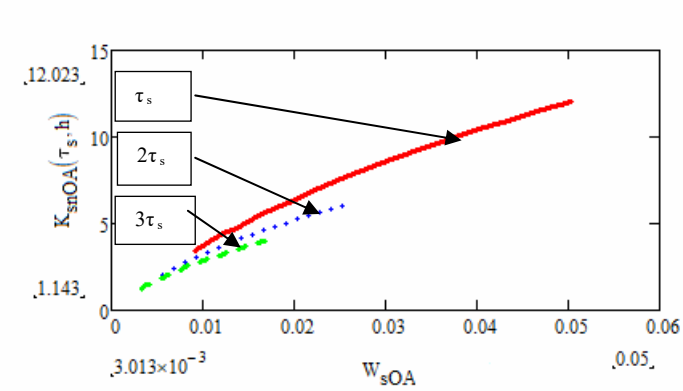

Figure 3. Effect of normal loud and correlation distance asperity on normal contact stiffness (OA model) for three correlation distance (τ)
——— τ_s=7.88x10^{-3}, - - - - - - - - $2\tau_s$=0.016, - - - - - - - - $3\tau_s$=0.024

In figure 4, the rigidity of a roughness surface is compared in the GW and OA models for rail-wheel roughness.

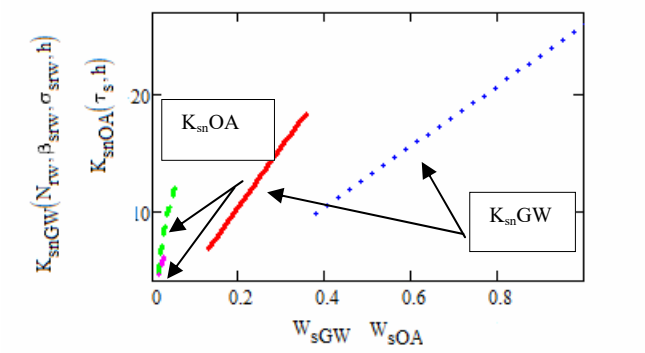

Figure 4. Effect of normal loud on normal contact stiffness (GW and OA models)
——— σ_{srw} = 0.019; , - - - - - - - - $2\sigma_{srw}$=0.038 , - - - - - - - - τ_s=7.88x10^{-3} - - - - - - - $2\tau_s$=0.016

3. Use of fractal parameters

The normal contact stiffness of the wheel-rail contact has an essential effect on dynamic characteristics. In the fractal contact stiffness model, based on elastic theory, the deformation of an asperity is carried out. From both Hertz contact theory and fractal theory is derived the contact area, contact stiffness and normal load and the effect of asperity interaction between wheel and rail on contact stiffness are studied by comparing with the fractal model. It is observed that the normal contact stiffness determines the mechanical properties of the wheel -rail contact [9].

On the other hand, normal contact stiffness has a close relationship with the roughness surface topography [10-13]. Majumdar and Bhushan developed a fractal contact model (M-B model) of roughness surfaces based on the fractal geometry theory [14].

The scale-independent parameters, used in G-W model, were used to study the contact area and the normal contact load in the M-B model [14, 15].

The effect of the interaction on the local deformation of one asperity was studied by using the Newton-Raphson iterative method and provided good results, and subsequent, Ciavarella implemented an improved G-W model that included interaction between asperities from elastic contact [16].

Referring to obtain one solution for stiffness contact, it needs to calculate the fractal parameters, the fractal dimension D, respectively the fractal topological parameter G. These could be obtained by the structure-function method [12, 18, 22, 26]:

$$S1(N,k)=\frac{1}{N-k}\sum_{i=1}^{N-k}\left(\frac{y1_{i+k}-y1_i}{10^3}\right)^2 \tag{14}$$

The incremental variance of the rough surface profile function z (x) is defined as the structure function [18], and it is obtained by:

$z(x)=G^{D-1}\sum_{n=n_1}^{\infty}\frac{\cos(2\pi\gamma^n x)}{\gamma^{n(2-D)}}=G^{D-1}L_f^{2-D}\left(\frac{\pi x}{L_f}\right)$, where 1<D<2, γ^n determines the frequency spectrum, $\gamma>1$, L_f is the length scale of a fractal. The possibility of asperity transition from elastic to plastic contact mode as its loading increases is determined with the critical area, that separates the elastic deformation from the plastic one [19], thus:

$$a_c(D,G,L_f,\phi)=\frac{1}{\pi}\left(\frac{k_e\phi}{2}\right)^2\left(\frac{L_f^D}{G^{D-1}}\right)^2 \tag{15}$$

where K_e = 3.2 is report of hardness (H) and yield strength of material (σ_y); elasticity parameter $\phi=\frac{\sigma_y}{E}$.

Using the following dimensionless $G_s=\frac{G}{(A_n)^{1/2}}$; $a_{cs}=\frac{a_c}{A_n}$ and, $A_{rs}=\frac{A_r}{A_n}$, where, A_n is the nominal area, A_c is critical area, A_{rs} is the dimensionless form of real contact area, G_s is the dimensionless topological fractal roughness parameter and ϕ represents the material property, the fractal contact model considering asperity interaction in a dimensionless static load W_{sW}, is given as:

$$Ec(\psi,D)=\psi^{\frac{2-D}{2}}-\left(1+\psi^{\frac{-D}{2}}\right)^{\frac{D-2}{D}}-\frac{(2-D)}{D} \tag{16}$$

and dimensionless normal load:

$$W_{sW}=\frac{4}{3(2\pi)^{1/2}}G_s^{D-1}\psi(D)^{\frac{2-D}{2}}A_{rs}^{\frac{3-D}{2}}\frac{D}{3-2D}\left[1-\frac{a_{cs}}{A_{rs}}^{\frac{3-2D}{2}}\right]+2.8\phi\left(\frac{D}{2-D}\right)^{\frac{2-D}{2}}A_{rs}^{\frac{D}{2}}a_{cs}^{\frac{2-D}{2}}\psi(D)^{\left(\frac{2-D}{2}\right)^2},$$

$D\neq 1.5$

$$W_{sW}=\frac{4}{3(2\pi)^{1/2}}G_s^{D-1}\psi(D)^{\frac{2-D}{2}}A_{rs}^{\frac{3-D}{2}}\frac{-D}{2}\left(\ln\frac{a_{cs}}{A_{rs}}\right)+8.4\phi\left(\frac{A_{rs}}{3}\right)^{\frac{3}{4}}a_{cs}^{\frac{1}{4}}\psi(D)^{\left(\frac{1}{16}\right)},D=1.5 \tag{17}$$

Afterwards, the relationship computed by Wang, between the normal contact load W_{sW} and the contact area A_{rs} of the roughness surface. For describe the size distribution function, the domain extension factor ψ was introduced, and it could be written by way of the equation [24].

Figures 5 a, b illustrate the variation of the dimensionless normal force with the fractal parameters D and G_s (Figure 5a for two values of the dimensionless critical area (a_{cs}) for separating the elastic deformations from the plastic ones (figure 5b).

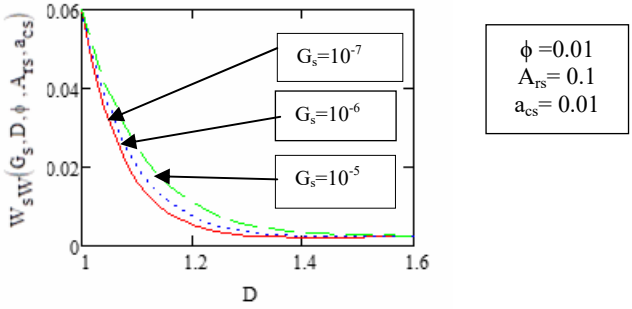

(a)

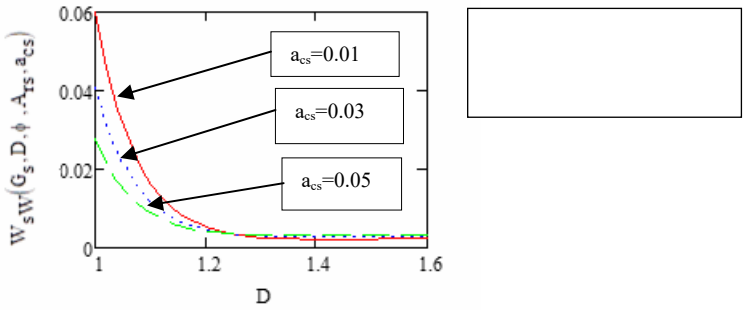

(b)

Figure 5. Dimensionless normal loud versus fractal parameter for different values of G_s (a) and different values of critical area (a_{cs})(b).

The real contact area is not only related to the normal load, but it also depends on the fractal parameters of contact surfaces, as noted in the figures 6 and 7.

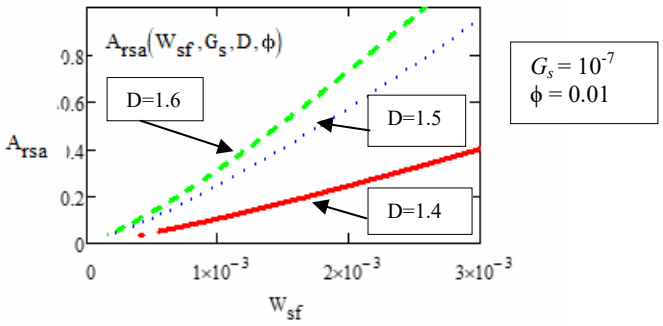

Figure 6. Real contact area versus normal loud for some fractal parameter (D).

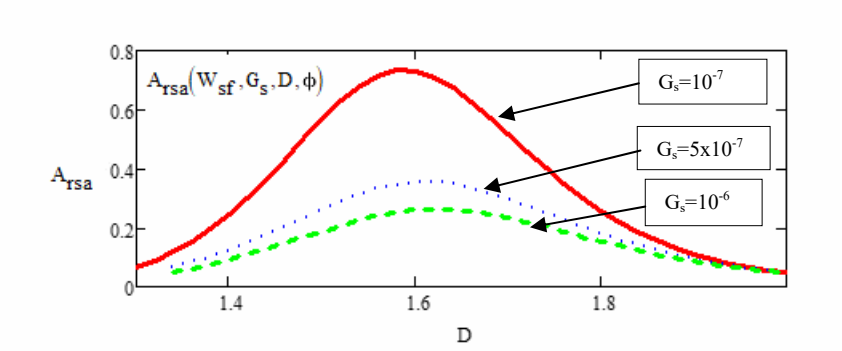

Figure 7. Real contact area versus fractal parameters (D, G_s).

From figure 7 it is observed the existence of a maximum of the real area with the variation of the fractal parameter D for three values of the topological fractal parameter G_s for W_{sf} = 0.002 and ϕ = 0.01.

The stiffness and damping of wheel-rail contact, both of which are affected by the preload, can be modelled based on the fractal contact theory. Thus, to compute the stiffness and damping coefficient the fractal parameters D and G were obtained using the roughness of the wheel/rail, determined with an m | rail trolley and m | wheel equipment. The connection between contact area A_r and normal contact stiffness (Wang model), $K_{sW,}$ of the wheel-rail contact, could be computed by the next equations:

$$K_{sW} = \frac{1}{(2\pi)^{1/2}} \frac{D}{1-D} \psi(D)^{\left(\frac{2-D}{2}\right)} A_{rs}^{1/2} \left[1 - \left(\frac{a_{cs}}{A_{rs}} \right)^{\frac{1-D}{2}} \right], \text{ where } K_{sW} = \frac{K_n}{E A_n^{1/2}} \quad (18)$$

Knowing the dependence of the real dimensionless area (A_{rs}) on the external normal force (load on the wheel) and the fractal characteristics of the rail and wheel surfaces (roughness on the contact ellipse), it is presented in figure 8 Kas_W dimensionless rigidity for different working conditions. Thus, in figure 8 can be observed the variation of the wheel and rail contact stiffness with the increase of the dimensional wheel load for the fractal parameters of the rail microgeometry, e.g. $Gsr = 1.74x10^{-8}$, Dr = 1.667 and of the wheel $Gsw = 1.3x10^{-6}$, respectively Dw = 1.472. Contact ellipse at nominal load was considered $Q = 69x10^3$ N ($Ws = 3.648 \times 10^{-3}$) has semiaxes a_H = 6.1 mm and b_H = 4.7 mm.

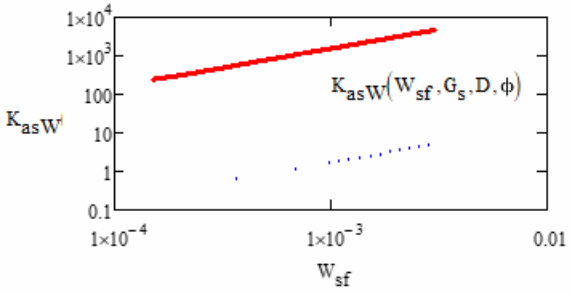

Figure 8. Normal rigidity (K_{asW}) versus normal load (W_{sf}) for fractal parameters of roughness of rail ($G_{sr,}$ D_r) and wheel ($G_{sr,}$ D_r).

In the hypothesis of changing the microgeometry of the rail and wheel roughness through wear processes (changing the fractal parameters, D and Gs), the contact stiffness changes significantly. For example, from figure 9 can be observed the increase of the rigidity with the increase of the parameters D and G_s at the dimensionless load on the wheel $W_s = 3.64x10^{-3}$ and the dimensionless

critical area $a_{cs} = 0.01$, the fractal parameters $G_{sr} = 1.74\text{x}10^{-8}$, $G_{sw} = 1.3\text{x}10^{-6}$.

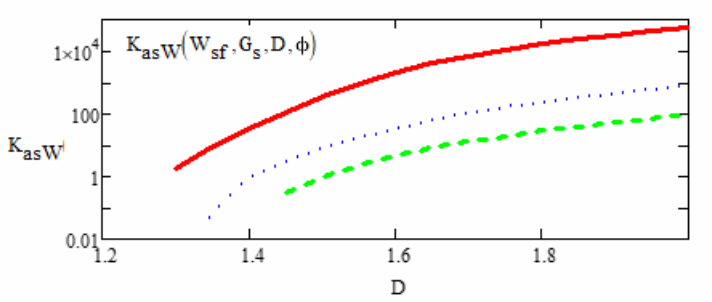

Figure 9. Normal rigidity (K_{asW}) versus fractal parameter (D) for fractal topological parameters of roughness of rail (G_{sr}), and wheel (G_{sr}).

During the transfer of the normal force from the wheel to the rail elastic and plastic deformations occur, depending on the sizes of the roughness and the elasticity and plasticity properties of the material. It is considered that it is important for the vibrations of the sine-wheel system to know the relation between the energy (mechanical work) for the elastic deformation (E_p) and the elastic deformation (E_e).

Taking into account the connection between the normal force and the elastic or plastic deformation, depending on the number of asperities of the contact area and the definition of the mechanical work, the report is deduced:

$$\eta_{pe} = \frac{15(2\pi)^{1/2}}{16} 2.8\phi \frac{5-3D}{2-D} G_s^{1-D} \left(\frac{a_{cs}}{A_{rs}}\right)^{2-D} \frac{1}{A_{rs}^{\frac{1-D}{2}} \left[1-\left(\frac{a_{cs}}{A_{rs}}\right)^{\frac{5-3D}{2}}\right]} \tag{19}$$

Substituting the real dimensionless area A_{rs} as a function of the normal force on the wheel and the fractal characteristics of the microgeometry and the critical area, deduces η_{ape} *(W_{pe}, G_s, D, φ).*
The energy efficiency of the contact is defined, (η_{at}) as the ratio between the mechanical work of the losses by plastic deformations and the total mechanical work.

$$\eta_{at} = \frac{\eta_{ape}}{1+\eta_{ape}} \tag{20}$$

Figure 10 illustrates the variation of this efficiency with the load on the wheel, for the continuous contact with the measured and analysed microgeometry.

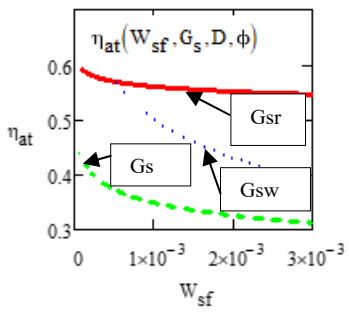

Figure 10. The energy efficiency of contact versus normal load on the wheel for fractal parameters of roughness for rail and wheel ($a_{cs} = 0.01$).
——— *Gsr* = $1.74\text{x}10^{-8}$ - - - - - - - - - Gsw = $1.3\text{x}10^{-6}$ - - - - - - - - - *Gs* = 10^{-7}

The microgeometry of the contact surfaces significantly influences the efficiency. Thus, in figure 10 the influence of the fractal parameter D is observed, for three values of the parameter Gs.

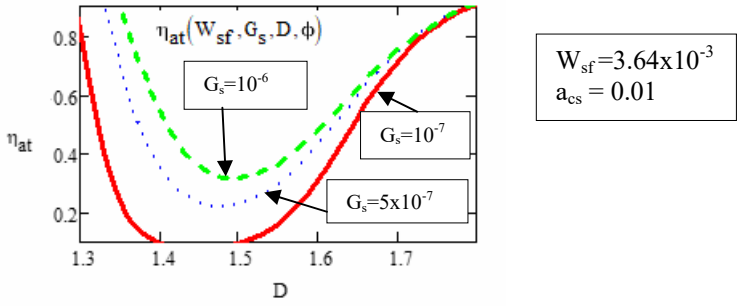

Figure 11. The energy efficiency of contact versus fractal parameter for the fractal parameter of roughness for rail and wheel.

Thus, can be observed the existence of a minimum efficiency (energy losses through plastic deformations) for values of the fractal parameter D between 1.4 and 1.6. The minimum yield value is dependent on the topological fractal parameter Gs.

4. Conclusion

When considering the GW model, the input data, the standard deviation σ, the mean effective radius of curvature β and the density of asperities η are defined, to estimate the contact stiffness.

It can be observed that a decrease of σ or β powerfully increases (under equal normal load) the contact stiffness, while the latter increases with increasing η.

When considering the OA model, the input data are the standard deviation σ and the correlation distance ($\tau\tau$). It is easy to conclude that reducing σ to half its value will double the amount of the contact stiffness K_n, the same load W and the same separation d, as can be concluded from equations (1) and (5).

In the GW model, the effect of σ on the contact stiffness is quite like its effect in the OA model.

Based on the OA model, results in a contact stiffness greater, than that obtained with the GW model. This discrepancy comes from the fact that the GW model underestimates the contact pressure since it uses asperities of constant curvature, while in the OA model the existence of a distribution of asperity curvature increases the contact pressure.

According to all these results, it is possible to increase the contact stiffness of a machine (which is substantially decreased by the existence of asperities) in two ways, either by using excellent contacting surfaces, which is expensive or by increasing the normal load, which mainly increases the state of stress of individual components.

As is shown in figure 6 with D and Gs increasing, the dimensionless normal contact stiffness monotonically increases and decreases respectively.

The increasing of the two fractal parameters, D and Gs, can be explained with the fact that the amplitude of surface topography is larger. In this case, can be achieved a larger contact area, which can provide a larger normal contact stiffness, as is shown in figure 6.

Based on the relation between contact stiffness and the fractal smoothness, it is found that in a specified interval, the smoother the contact surface is, the higher the stiffness is. But when the fractal smoothness reaches a specific value, increasing it will reduce contact stiffness instead. The main reason for this trend is that the effect of the surface smoothness on the normal contact stiffness can be offset by the asperity interaction.

Based on the fractal model, which considers the asperity interaction, the deformation of an asperity was studied can be concluded that:

- considering the independent variable as real contact area or normal load, in the simulation range, the normal contact stiffness is proportional with the fractal dimension D and indirectly proportional with the fractal roughness parameter G.
- the effect of the asperity interaction on the normal contact stiffness can be accomplished by increasing the normal load and the fractal dimension D and decreasing fractal roughness parameter G will increase.
- Considering the relation between D, G and surface roughness, the definition of fractal smoothness S_f was proposed. It has a clear physical interpretation: the greater the fractal smoothness, the smoother the surface.

The reason is that with the normal load increasing, two small adjacent asperities are joint into a larger hardness, which also can lead to the continuous increase of the actual contact area between surfaces.

5. References

[1] Xiao H F, Sun Y Y and Xu J W 2018 Investigation into the normal contact stiffness of rough surface in line contact mixed elastohydrodynamic lubrication *Tribology Transactions* **61** pp 742–753
[2] Xiao F and Sun Y 2019 On the normal contact stiffness and contact resonance frequency of rough surface contact based on asperity micro-contact statistical models *European Journal of Mechanics / A Solids* **75** pp 450–460
[3] Sherif H A 1991 Parameters affecting contact stiffness of nominally flat surfaces *Wear* **145** pp 113-121
[4] Shi X and Polycarpou AA 2005 Measurement and modelling of normal contact stiffness and contact damping at the meso scale *Journal of Vibration and Acoustics* **127** pp 52–60
[5] Zhao Y W, Maietta D M and Chang L 2000 An asperity microcontact model incorporating the transition from elastic deformation to fully plastic flow *ASME Journal Tribology* **122** pp 86–93
[6] Greenwood J A, Williamson J B P. 1966 Contact of nominally flat surfaces. *Proc R Soc LondonSer A* 295 pp 300–319.
[7] Whitehouse D J and Archard A F 1970 The properties of random surfaces of significance in their contact Proc. *R. Sot. A,* 316 pp 97-121.
[8] Onions R A and Archard A F 1973 The contact of surfaces having a random structure, *Journal Physis* **6** pp 289-304.
[9] Pan W, Li X, Wang L, Guo N and Mu J 2017 A normal contact stiffness fractal prediction model of dry-friction rough surface and experimental verification *European Journal of Mechanics / A Solids* **66** pp 94-102.
[10] Popov V L 2010 Contact Mechanics and Friction *Springer* pp 81-103.
[11] Zhu L, Li H and Wang W 2013 Research on rotary surface topography by orthogonal turn-milling *The International Journal of Advanced Manufacturing Technology* **69** pp 2279-2292
[12] Zhai C, Gan Y, Hanaor D, et al. 2015 The Role of Surface Structure in Normal Contact Stiffness Experimental Mechanics **56** pp 1-10.
[13] Pohrt R and Popov V L 2012 Normal contact stiffness of elastic solids with fractal rough surfaces *Physical Review Letters* **86** 104301
[14] Majumdar A and Bhushan B 1991 Fractal model of elastic-plastic contact between rough surface *ASME Journal Tribology* **113** pp 1–11
[15] Bhushan B and Majumdar A 1992 Elastic-plastic contact model for bifractal surfaces *Wear* **153** pp 53–64
[16] Ciavarella M, Greenwood JA and Paggi M 2008 Inclusion of interaction in the Greenwood and Williamson contact theory *Wear **265*** pp 729-734
[17] Sherif H A 1991 Parameters affecting contact stiffness of nominally flat surfaces *Wear **145***

pp 113-121
[18] Ganti S and Bhushan B 1995 Generalized fractal analysis and its applications to engineering surfaces *Wear* **180** pp 17-34.
[19] Morag Y and Etsion I 2007 Resolving the contradiction of asperities plastic to elastic mode transition in current contact models of fractal rough surfaces *Wear* **262** pp 624-629
[20] Yan W and Komvopoulos K 1998 Contact analysis of elastic-plastic fractal surfaces *Journal Appl. Phys*. **84** pp 3617-3624
[21] Greenwood JA and Tripp JH 1971 The contact of two nominally flat rough surfaces. *Proc Inst Mech Engrs* **185** pp 624–33
[22] Majumdar A, and Tien C L 1990 Fractal Characterization and Simulation of Rough Surfaces *Wear* vol. **136** pp. 313-327
[23] Wang S and Komvopoulos K 1994 A fractal theory of the interfacial temperature distribution in the slow sliding regime. Part I: elastic contact and heat transfer analysis *Journal Tribology-T ASME* **116** pp 812-823
[24] Wang F, Ho SCM, Huo L and Song G 2018 A novel fractal contact-electromechanical impedance model for quantitative Monitoring of Bolted Joint loosenes *IEEE*
[25] J. Pullen and J. B. P. Williamson 1973 On the plastic contact of rough surfaces, Proc. *R. Sot. A,* **327** pp 159-173.
[26] Babici L M and Tudor A 2019 Some aspects regarding the roughness of the railway surface and rolling noise at locomotives, *IOP Conf. Series: Materials Science and Engineering,* **514**